

# Warisan Journal of Mathematical Sciences and Engineering

Journal homepage: https://warisanunggul.my/index.php/wjmse/index ISSN: 3093-6896



## Analytical Study of Velocity and Dispersion Function in Unsteady Non-Newtonian Blood Flow with Chemical Reaction in a Straight Artery

Reaswina Kusraju<sup>1</sup>, Nurul Aini Jaafar<sup>1,\*</sup>, Mallinath Dhange<sup>2,3</sup>

- 1 Department of Mathematical Sciences, Faculty of Science, Universiti Teknologi Malaysia, 81310 Skudai, Johor, Malaysia
- Department of Mathematics BLDEA's VP Dr. PG Halakatti College of Engineering and Technology, Vijayapur,586103 India (Affiliated to Visvesvaraya Technological University, Belagavi, Karnataka, India)
- 3 Department of Allied Health Sciences, Shri B.M. Patil Medical College, Hospital and Research Centre, BLDE (Deemed to be University), Vijayapur, India

#### **ARTICLE INFO**

#### **ABSTRACT**

#### Article history:

Received 25 July 2025 Received in revised form 18 August 2025 Accepted 25 September 2025 Available online 21 October 2025 Accurate drug delivery in stenosed arteries is influenced by blood flow dynamics, particularly velocity distribution and solute dispersion. This study investigates unsteady solute transport in a non-Newtonian Casson fluid through a straight artery with symmetric stenosis, emphasizing the effects on velocity and dispersion function. Using the Generalized Dispersion Model (GDM), the governing equations are solved to assess how variations in plug flow region, height of stenosis, length of the stenosed area, length from the origin till the stenosed section and the axial position impacts the blood flow characteristics. Results indicate that the presence of stenosis significantly reduces axial velocity due to increased yield stress, especially near the arterial walls. The dispersion function exhibits a declining trend in these regions, suggesting limited solute spread, whereas higher dispersion is observed at the arterial center. The interplay between yield stress and stenosis geometry contributes to complex dispersion behavior, offering insights into convective-diffusive transport under physiological conditions. This analysis enhances understanding of solute dynamics in stenosed vessels, with implications for optimizing targeted drug delivery strategies.

#### Keywords:

Casson fluid; non-Newtonian; blood flow; Generalized Dispersion Model; chemical reaction

#### 1. Introduction

The analysis of blood flow through arterial segments has long been a focus in hemodynamics, particularly when studying pathological conditions such as stenosis. Due to the complex rheological nature of blood, it is often modeled as a non-Newtonian fluid. Among several non-Newtonian models, the Casson fluid model, introduced by Casson [1], has proven particularly effective in capturing blood's yield stress and shear-thinning characteristics. This model has been widely adopted to simulate blood flow in both normal and constricted arteries. Gill [2] developed an analytical method to solve transient dispersion problems in fully developed laminar flow within a tube. Using a series solution, he described how solute concentration changes over time and space. This approach

E-mail address: nurulaini.jaafar@utm.my

https://doi.org/10.37934/wjmse.2.1.2649

26

<sup>\*</sup> Corresponding author.

extended Taylor's dispersion theory and provided a simpler way to handle more complex flow and boundary conditions.

Early work by Haldar [3] provided foundational insights into pulsatile blood flow in stenosed arteries, motivating further studies that incorporate the Casson model into vascular simulations. Siddiqui *et al.*, [4] emphasized the relevance of using non-Newtonian models to analyze blood flow through irregular geometries such as stenosed vessels. Building on this, Chakravarty and Mandal [5] examined flow in tapered arteries with stenosis using a layered Casson model, demonstrating the impact of pressure gradients and wall behavior on flow dynamics.

Chemical reactions occurring within the bloodstream also play a crucial role in altering solute concentration and transport. When integrated into fluid dynamic models, such reactions influence the dispersion of drugs and other transported substances. Recent studies, such as those by Beg and Roy [6], have incorporated chemical reaction terms into the governing equations to better represent drug delivery scenarios within stenosed arteries.

Al-Kalbani et al., [7] focuses on solute dispersion in a straight stenosed artery using the Casson fluid model with the influence of chemical reactions, similar to the present study. However, his analysis is conducted under steady-state conditions and uses the Taylor-Aris dispersion theory, whereas the current study addresses unsteady flow and applies the Generalized Dispersion Model (GDM). Thus, while both studies share the same fluid model and artery geometry, mine offers a more dynamic representation by capturing time-dependent dispersion behavior. Jaafar et al., [8] investigates unsteady solute dispersion using the GDM, aligning with the time-dependent nature of my research. However, the author uses a Bingham fluid model instead of Casson fluid, considers overlapping stenoses, and excludes chemical reaction effects. In contrast, the present study maintains a straight stenosed artery, incorporating chemical reactions, and uses the Casson model, making it more reflective of actual blood rheology under pathological conditions. Raj et al., [9] presented a mathematical investigation of solute dispersion in non-Newtonian blood flow through a stenosed artery under the influence of a chemical reaction, employing the Casson fluid model. Their approach centered on obtaining approximate analytical solutions using the Adomian Decomposition Method (ADM), with particular emphasis on analyzing the velocity and solute concentration profiles. While their study shares common ground with the present work in terms of fluid model, arterial stenosis, and chemical reactivity, the scope and methodology differ significantly.

Besides, Jaafar et al., [10] investigated the unsteady dispersion of a solute in blood flow in the presence of a first-order chemical reaction. In this study, blood was modelled as a non-Newtonian Casson fluid to reflect its realistic flow behaviour under physiological conditions. The analysis was carried out using the generalized dispersion model (GDM), which was applied to two flow geometries, a circular pipe and a parallel plate channel. The main objective was to understand how chemical reactions and vessel geometry influence the dispersion function and relative axial diffusivity over time. Dhange et al., [11] investigated the effect of a forced field on blood flow through an artery with overlapping stenosis. Blood was modeled as a Casson fluid, and the artery was treated as an inclined, axisymmetric tube. The study analytically examined velocity, flow resistance, and wall shear stress under varying field strengths, stenosis heights, and inclination angles, highlighting the influence of external forces on hemodynamics in diseased arteries. Dhange et al., [12] analyzed the hemodynamic properties of blood flow in an angled artery with overlapping stenosis, incorporating the effects of a force field and suspended gold nanoparticles. Blood was modeled as a non-Newtonian nanofluid, and the study focused on evaluating velocity, temperature distribution, wall shear stress, and flow resistance. The results demonstrated that both the external force field and gold nanoparticle suspension significantly influence flow behavior, offering potential improvements in therapeutic flow regulation. Elias et al., [13] studied the dispersion of solute in a Casson fluid flowing

through a stenosed artery under the influence of body acceleration and velocity slip at the arterial wall. Using the generalized dispersion model, they derived expressions for the velocity profile, dispersion function, and mean concentration. Their findings showed that increased body acceleration and slip conditions enhance solute transport and reduce flow resistance, offering insights into controlled drug delivery under physiological forces.

Current studies rarely integrate unsteady flow, Casson fluid behavior, and chemical reactions within a single model to analyze solute dispersion in stenosed arteries. Most existing work either assumes steady-state conditions, uses different fluid models, or neglects the impact of reaction kinetics. There is limited analytical research applying the Generalized Dispersion Model (GDM) to capture the combined effects of these parameters in a straight artery with symmetric stenosis.

Drug delivery in patients with arterial stenosis remains a clinical challenge due to altered blood flow patterns and complex solute transport mechanisms. In particular, the presence of chemical reactions and the non-Newtonian nature of blood significantly affect the velocity distribution and dispersion of solutes within narrowed arteries. These factors, combined with geometric variations in stenosed segments, complicate the prediction of drug movement. To improve targeted treatment strategies, it is essential to conduct a detailed analytical study on how velocity and dispersion are influenced under unsteady flow conditions. The main objective of this study is the need for a comprehensive understanding of solute behavior in non-Newtonian blood flow with chemical reactions, focusing on a straight artery with symmetric stenosis. The Generalized Dispersion Model (GDM) is used to derive and evaluate the dispersion function, which quantifies axial solute spreading. Key variables investigated include the plug flow region, height of stenosis, length of the stenosed area, distance from the origin to the stenosed section, and the axial position. Analytical and graphical results are obtained in order to offer insights on how these parameters influence solute dispersion and transport efficiency in physiologically relevant arterial geometries.

### 2. Methodology

#### 2.1 Mathematical Formulation

This investigation is conducted within a two-dimensional rigid tube framework, incorporating the effects of chemical reactions. This encompasses research about the flow characteristics of Casson's fluid and the dispersion of solutes in the context of non-Newtonian blood flow. The focus is on velocity and dispersion functions of blood flow. This research additionally encompasses the analysis of unsteady behavior of solute within non-Newtonian fluids that undergo chemical reactions.

Figure 1 shows the geometry for a straight stenosed artery in the bloodstream using the cylindrical polar coordinate system  $(\overline{r},\overline{\psi},\overline{z})$  where the artery design for the Casson fluid model with stenosis where  $\overline{w}$  is the axial velocity,  $\overline{z}$  is the axial coordinate,  $\overline{R}_0$  is the radius of artery,  $\overline{\psi}$  is the azimuthal angle,  $\overline{r}_p$  is the radius of the plug flow region in circular artery and  $\overline{L}$  is the length of the solute,  $\overline{R}(\overline{z})$  represents the radius of the stenosed segment between the stenosed area and plug flow region at the axial position  $\overline{z}$ ,  $\overline{d}$ ' is the length from the origin till the stenosed section,  $\overline{l}_0$  is the length of stenosed area,  $\overline{z}_1$  represents the point at axial position  $\overline{z}$  at Cartesian coordinate and  $\overline{\delta}$  is the maximum height of stenosis. A stenosis with symmetry above and below the central axis is depicted in the Figure 1, which causes a consistent narrowing in the radial direction.

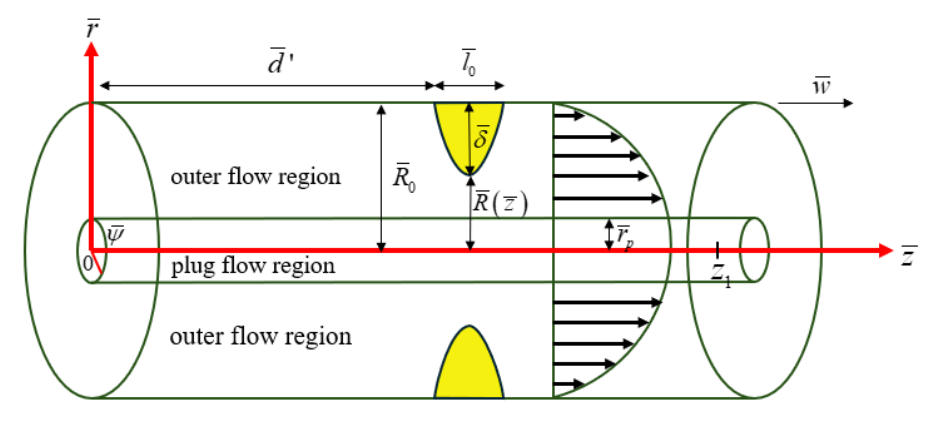


Fig. 1. The geometry for a straight stenosed artery

## 2.2 Momentum Equation

The momentum equation for steady flow is defined as below:

$$\frac{1}{\overline{r}}\frac{d}{d\overline{r}}(\overline{r}\,\overline{\tau}) = -\frac{d\overline{p}}{d\overline{z}},\tag{1}$$

where  $\bar{r}$ ,  $\bar{\tau}$ ,  $\bar{\tau}_y$ ,  $\bar{p}$  and  $\bar{z}$  and  $\frac{d\bar{p}}{d\bar{z}}$  are plug core radius, shear stress, yield stress, pressure, axial distance and pressure gradient in dimensional form.

The boundary condition of Eqn (1) is given as follows:

$$\bar{\tau}$$
 is finite at  $\bar{r}$  = 0. (2)

## 2.3 Governing Equation

The constitutive equation for a Casson fluid is given by Jaafar et al. [10] as follows:

$$-\frac{d\overline{w}}{d\overline{r}} = \begin{cases}
\frac{1}{\overline{\mu}} \left( \sqrt{\overline{\tau}} - \sqrt{\overline{\tau}_y} \right)^2 & \text{if } \overline{\tau} > \overline{\tau}_y, \\
0 & \text{if } \overline{\tau} \le \overline{\tau}_y,
\end{cases} \tag{3}$$

where  $\overline{\mu}$  is the viscosity coefficient of Casson fluid with  $M\!L^{\!-\!1}T^{\!-\!1}$  dimension and  $\overline{\tau}_y$  is the yield stress. When  $\overline{\tau}_y=0$ , the Casson fluid model reduces to then Newtonian fluid model. The central region of the artery is referred to as the plug flow area, also known as the plug core region when  $\overline{\tau} \leq \overline{\tau}_y$ . For unknown velocity  $\overline{w}$ , no slip at the wall of the circular pipe creates the no slip boundary condition as follows:

$$\overline{w} = 0$$
 at  $\overline{r} = \overline{R}(\overline{z})$ , (4)

where

$$\overline{R}(\overline{z}) = \begin{cases}
\overline{R}_{0}, & 0 \leq \overline{z} \leq \overline{d}', \\
\overline{R}_{0} - \frac{4\overline{\delta}}{\overline{l}_{0}^{2}} \left(\overline{l}_{0} \left(\overline{z} - \overline{d}'\right) - \left(\overline{z} - \overline{d}'\right)^{2}\right), & \overline{d}' \leq \overline{z} \leq \overline{d}' + \overline{l}_{0}, \\
\overline{R}_{0}, & \overline{d}' + \overline{l}_{0} \leq \overline{z} \leq \overline{z}_{1},
\end{cases} \tag{5}$$

where  $\overline{R}(\overline{z})$ ,  $\overline{R}_0$ ,  $\overline{l}_0$ ,  $\overline{d}$ ,  $\overline{\delta}$  and  $\overline{z}_1$  represents the radius of the stenosed segment, radius of the artery without stenosis, the length of stenosis and the distance from the origin, the maximum height of stenosis and the point at axial axis in  $\overline{z}$  direction.

## 2.3.1 Convective diffusion coefficient

The two-dimensional unsteady convective-diffusion equation of solute concentration similar to Debnath *et al.* [14] and Roy and Beg [15] in cylindrical coordinate system is given as

$$\frac{\partial \bar{C}}{\partial \bar{t}} + \bar{w} \frac{\partial \bar{C}}{\partial \bar{z}^*} = \bar{D}_m \left( \bar{l}^2 + \frac{\partial^2}{\partial \bar{z}^{*2}} \right) \bar{C} - \bar{\alpha} \bar{C}, \tag{6}$$

where

$$\overline{l}^{2} = \frac{1}{\overline{r}} \frac{\partial}{\partial \overline{r}} \left( \overline{r} \frac{\partial}{\partial \overline{r}} \right), \tag{7}$$

where  $\bar{C}$  is the concentration of solute in components and  $\bar{D}_{\scriptscriptstyle m}$  is the molecular diffusion. According to Gill and Sankarasubramanian [16] stated the initial condition for (6) and (7) , for component  $\bar{C}$  is as below,

$$\overline{C}(\overline{r}, \overline{z}^*, 0) = \begin{cases}
\overline{C}_0 & \text{if } |\overline{z}^*| \leq \frac{\overline{z}_s}{2}, \\
0 & \text{if } |\overline{z}^*| > \frac{\overline{z}_s}{2}.
\end{cases} \tag{8}$$

The boundary conditions for component  $\bar{C}$  for (6) and (7), given by

$$\overline{C}(\overline{r}, \infty, \overline{t}) = 0, \tag{9}$$

for symmetry at the centre of a circular pipe  $\overline{r} = 0$ , the boundary condition for (6) and (7) is given by

$$\frac{\partial \overline{C}}{\partial \overline{r}}(0,\overline{z}^*,\overline{t}) = 0 \tag{10}$$

and  $\overline{r} = \overline{R}(\overline{z})$  for solute concentration gradient at the wall, the boundary condition for (6) and (7) is given by

$$\frac{\partial \overline{C}}{\partial \overline{r}} \left( \overline{R}(\overline{z}), \overline{z}^*, \overline{t} \right) = 0. \tag{11}$$

#### 2.3.2 Non-dimensional variables

The non-dimensional variables are referred to Dash *et al.* [17], Sankar and Lee [18] and Sebastian and Nagarani [19] as the following:

$$r = \frac{\overline{r}}{\overline{R}_{0}}, \quad z = \frac{\overline{z}}{\overline{R}_{0}}, \quad P = \frac{\overline{P}\overline{\mu}\overline{w}_{0}}{\overline{R}_{0}}, \quad R(z) = \frac{\overline{R}(\overline{z})}{\overline{R}_{0}}, \quad \tau = \frac{\overline{\tau}\overline{R}_{0}}{\overline{\mu}\overline{w}_{0}}, \quad \tau_{y} = \frac{\overline{\tau}_{y}\overline{R}_{0}}{\overline{\mu}\overline{w}_{0}},$$

$$w = \frac{\overline{w}}{\overline{w}_{0}}, \quad t = \frac{\overline{D}_{m}\overline{t}}{\overline{R}_{0}^{2}}, \quad r_{p} = \frac{\overline{r}_{0}}{\overline{R}_{0}}, \quad C = \frac{\overline{C}}{\overline{C}_{0}}, \quad z^{*} = \frac{\overline{D}_{m}\overline{z}^{*}}{\overline{R}_{0}^{2}\overline{w}_{0}}, \quad z_{s} = \frac{\overline{D}_{m}\overline{z}_{s}}{\overline{R}_{0}^{2}\overline{w}_{0}},$$

$$l_{0} = \frac{\overline{l}_{0}}{\overline{R}_{0}}, \quad \delta = \frac{\overline{\delta}}{\overline{R}_{0}}, \quad d' = \frac{\overline{d}'}{\overline{R}_{0}}, \quad \alpha = \sqrt{\frac{\overline{R}_{0}^{2}\overline{\alpha}}{\overline{D}_{m}}},$$

$$(12)$$

where  $\overline{w}_0$ , r,  $\tau$ ,  $\tau_y$ , R(z),  $\overline{P}$ , z, w,  $r_p$ , C,  $l_0$ ,  $\delta$  and d are fluid characteristic velocity, plug core radius, radial direction, shear stress, yield stress, stenosed radius, pressure, axial distance, velocity in the  $\overline{z}$  direction, radius of the artery in plug flow region, solute concentration, length of the stenosed area, height of stenosis and length from the origin till the stenosed section.

#### 2.3 Method of Solution

By using non-dimensional variables in Eqn (12) into Eqn (1) and Eqn (2), the momentum equation and boundary condition are given as follows

$$\frac{d(\tau r)}{dr} = r \left[ -\frac{dp}{dz} \right] \tag{13}$$

and

$$\tau$$
 is finite at  $r = 0$ . (14)

The outcome of shear stress is obtained by integrating Eqn (13) with respect to r using the boundary condition in Eqn (14) as follows

$$\tau = \frac{r}{2} \left[ -\frac{dp}{dz} \right]. \tag{15}$$

By using non dimensional variables of Eqn (12) into Eqn (3) until Eqn (5), the non-dimensional variable of constitutive equation of Casson fluid is obtained as follows

$$-\frac{du}{dr} = \tau + \tau_y - 2\sqrt{\tau}\sqrt{\tau_y} \qquad \text{if } \tau > \tau_y$$
 (16)

$$w = 0 \text{ at } r = R(z), \tag{17}$$

where

$$R(z) = \begin{cases} 1, & 0 \le z \le d', \\ 1 - \frac{4\delta}{l_0^2} \left( l_0 \left( z - d' \right) - \left( z - d' \right)^2 \right), & d' \le z \le d' + l_0, \\ 1, & d' + l_0 \le z \le z_1. \end{cases}$$
(18)

By integrating Eqn (13) with respect to r by substituting Eqn (15) into Eqn (16) subject to Eqn (17), the velocity in the outer non-plug core region is obtained as follows:

$$w(r) = -\frac{1}{2} \left[ -\frac{dp}{dz} \right] \left[ R^2(z) - r^2 + 2(R(z) - r)r_p - \frac{8}{3}\sqrt{r_p} \left( R^{\frac{3}{2}}(z) - r^{\frac{3}{2}} \right) \right].$$
 (19)

Evaluating  $r = r_{_{D}}$  in the Eqn (19), the velocity in the plug flow region is shown as follows:

$$w(r_p) = -\frac{1}{2} \left[ -\frac{dp}{dz} \right] \left[ R^2(z) - r_p^2 + 2(R(z) - r_p) r_p - \frac{8}{3} \sqrt{r_p} \left( R^{\frac{3}{2}}(z) - r_p^{\frac{3}{2}} \right) \right].$$
 (20)

Mean velocity is solved using integral method by using Eqn (19) and Eqn (20), which then is formed as follows:

$$w_{m} = \frac{1}{8} \left[ -\frac{dp}{dz} \right] \left[ 1 + \frac{4}{3} r_{p} R(z) - \frac{16}{7} \sqrt{r_{p}} R^{\frac{3}{2}}(z) - \frac{1}{21} \frac{r_{p}^{4}}{R^{2}(z)} \right].$$
 (21)

The relative velocity in the plug core region,  $w_1 = w(r_p) - w_m$  and the relative velocity in outer core region,  $w_2 = w(r) - w_m$  are given by

$$w_{1} = \frac{R^{2}(z)}{8} \left[ -\frac{dp}{dz} \right] \left[ 1 - \frac{2}{3} r_{p}^{2} R(z) + \frac{8}{3} r_{p} - \frac{64}{21} r_{p}^{\frac{1}{2}} + \frac{1}{21} r_{p}^{4} \right], \tag{22}$$

$$w_{2} = \frac{R^{2}(z)}{8} \left[ -\frac{dp}{dz} \right] \left[ 1 - 2r_{p}^{2} + \frac{8}{3}r_{p} - 4rr_{p} - \frac{64}{21}\sqrt{r_{p}} + \frac{16}{3}\sqrt{r_{p}}r^{\frac{3}{2}} + \frac{1}{21}r_{p}^{4} \right].$$
 (23)

Using non-dimensional variables of Eqn (12) into Eqn (6) until Eqn (11) to yield as follows

$$\frac{\partial C}{\partial t} + w \frac{\partial C}{\partial z} = \left(l^2 + \frac{1}{Pe^2} \frac{\partial^2}{\partial z^2}\right) C - \alpha^2 C \tag{24}$$

where

$$Pe = \frac{R_0 u_0}{D_m}, \tag{25}$$

Pe is the Peclet number for the flow in a circular artery which is given by Dash et al. [17] and Ramana et al. [20], and

$$l^2 = \frac{1}{r} \frac{\partial}{\partial r} \left( r \frac{\partial}{\partial r} \right). \tag{26}$$

Next, the initial condition in non-dimensional variable, for component C is as below,

$$C(r,z^*,0) = \begin{cases} 1 \text{ if } |z^*| \le \frac{z_s}{2}, \\ 0 \text{ if } |z^*| > \frac{z_s}{2}, \end{cases}$$
 (27)

the boundary conditions are given by

$$C(r,\infty,t) = 0, (28)$$

for symmetry at the centre of a circular artery r=0, the boundary condition is given by

$$\frac{\partial C}{\partial r}(0, z^*, t) = 0 \tag{29}$$

and r = R(z) for solute concentration gradient at the wall, the boundary condition is given by

$$\frac{\partial C}{\partial r}(R(z), z^*, t) = 0. \tag{30}$$

By using approach of Gill and Sankarasubramanian [16] and by assuming the solution of Eqn (24) as a derivative series expansion involving  $\frac{\partial^i C_m}{\partial z_1^i}$  is shown as follows:

$$C(r,z,t) = C_m(z_1,t) + \sum_{i=1}^{\infty} f_i(r,t) \frac{\partial^i C_m(z_1,t)}{\partial z_i^i},$$
(31)

where  $C_{_m}$  is the mean concentration of the solute over a cross-sectional area of the geometry,  $f_i(r,t)$  is the dispersion function associated with  $\frac{\partial^i C_{_m}}{\partial z_1^i}$ .

## 2.3.1 Generalized Dispersion Model (GDM)

Generalized Dispersion Model (GDM) is a derivative series expansion of the approach of Gill and Sankarasubramanian [16] which is given as

$$\frac{\partial C_m}{\partial t} (z_1, t) = \sum_{i=1}^{\infty} K_i(t) \frac{\partial_i C_m}{\partial z_1^i} (z_1, t) - \alpha^2 C_m, \tag{32}$$

where  $K_i(t)$  is the transport coefficient derived as

$$K_{i}(t) = \frac{\delta_{i2}}{Pe^{2}} + 2\frac{\partial f_{i}}{\partial r}(1,t) - 2\int_{0}^{R(z)} f_{i=1}(r,t)u(r)rdr ; i = 1,2,3,...$$
 (33)

with the Kronecker delta,  $\delta_{ii}$  stated as

$$\delta_{ij} = \begin{cases} 0 & \text{if } i \neq j, \\ 1 & \text{if } i = j. \end{cases}$$
(34)

According to Eqn (33),  $K_1(t)$  is the longitudinal convection coefficient and  $K_2(t)$  is the longitudinal diffusion coefficient. When  $\alpha=0$ , it is observed that Eqn (32) is the same as stated by Gill and Sankarasubramanian [16].

#### 2.3.2 Dispersion function's governing equation

The infinite system of partial differential equations is given by substituting Eqn (32) into Eqn (24) and then equating the coefficients of  $\frac{\partial^i C_m}{\partial z_i^i}$  to zero for i=1,2,3,... as follows

$$\frac{\partial f_1}{\partial t} - \ell^2 f_1 + w - w_m + K_1(t) + \alpha^2 f_1 = 0,$$
(35)

$$\frac{\partial f_2}{\partial t} - \ell^2 f_2 + \left[ w - w_m + K_1(t) \right] f_1 + K_2(t) - \frac{1}{Pe^2} + \alpha^2 f_2 = 0$$
 (36)

and

$$\frac{\partial f_{i+2}}{\partial t} - \ell^2 f_{i+2} + \left[ w - w_m + K_1(t) \right] f_{i+1} + \left[ K_2(t) - \frac{1}{Pe^2} \right] f_i + \alpha^2 \sum_{j=2}^{i+2} K_j(t) f_{i+2-j} = 0$$
(37)

for i = 1, 2, 3, ...

The initial and boundary conditions of  $C(r, z_1, t)$  is implied that  $f_i$  must satisfied the following initial and boundary conditions given by Gill and Sankarasubramanian [16].

$$f_i(r,0) = 0 (38)$$

$$\frac{\partial f_i}{\partial r}(0,t) = 0 \tag{39}$$

and

$$\frac{\partial f_i}{\partial r} [R(z), t] = 0, \tag{40}$$

respectively.

The dispersion function  $f_1(r,t)$  is the coefficient of  $\frac{\partial C_m}{\partial z_1}$  which plays an important role in measuring

the deviation of the local concentration  $C(r,z_1,t)$  from the mean concentration  $C_m(z_1,t)$ . The solution of the Eqn (35) satisfying the boundary conditions from Eqn (38) – Eqn (40) and can be separated into two following parts, (Gill & Sankarasubramanian) [16]

$$f_1(r,t) = f_{1s}(r) + f_{1t}(r,t)$$
, (41)

where  $f_{1s}(r)$  is the dispersion function in the steady state and  $f_{1t}(r,t)$  is the dispersion function in the unsteady state that describes the time dependent nature of the dispersion of the solute. Applying Eqn (41) in Eqn (35) yields,

$$\frac{\partial f_{1s}}{\partial t} + \frac{\partial f_{1t}}{\partial t} - \ell^2 (f_{1s} + f_{1t}) + (w - w_m) + \alpha^2 (f_{1s} + f_{1t}) = 0.$$
 (42)

Grouping the  $f_{1s}(r)$  and  $f_{1t}(r,t)$  terms together and equating each of these to zero, obtain the respective simplified differential equations of  $f_{1s}(r)$ , the terms of  $\frac{\partial f_{1s}}{\partial t}$  in Eqn (42) is equal to zero for steady dispersion of solute as shown below

$$\ell^2 f_{1s} - (w - w_m) - \alpha^2 f_{1s} = 0 \tag{43}$$

and  $f_{1t}(r,t)$  as given by follows:

$$\frac{\partial f_{1t}}{\partial t} = \ell^2 f_{1t} - \alpha^2 f_{1t}. \tag{44}$$

Substituting Eqn (41) into conditions Eqn (38) – Eqn (40), and grouping  $f_{1s}(r)$  and  $f_{1t}(r,t)$  terms together, the initial condition of  $f_{1t}(r,t)$  is given by

$$f_{1t}(r,0) = -f_{1s}(r) \tag{45}$$

and the boundary conditions of  $f_{1s}(r)$  and  $f_{1t}(r,t)$  are given as follows:

$$\frac{df_{1s}}{dt}(0) = 0, (46)$$

$$\frac{df_{1s}}{dt}R(z)=0, (47)$$

$$\frac{df_{1t}}{dt}(0,t) = 0, (48)$$

and

$$\frac{df_{1t}}{dt}(R(z),t) = 0. (49)$$

Equating the solvability of  $f_{1s}(r)$  and  $f_{1t}(r,t)$ , the following solvability conditions for  $f_{1s}(r)$  and  $f_{1t}(r,t)$ , are as follows, (Gill and Sankarasubramanian) [16]

$$-\int_{0}^{R(z)} f_{1s} r dr = 0, (50)$$

$$\int_{0}^{R(z)} f_{1t} r dr = -\int_{0}^{R(z)} f_{1s} r dr.$$
 (51)

By integrating Eqn (43) with respect to r using boundary condition Eqn (46), Eqn (47) and Eqn (50), the solution of the steady dispersion function in the plug flow region is given by

$$f_{1s-}(r_p) = -\frac{1}{\alpha^2} \left( \frac{2}{(n+3)} + \frac{2(n+1)}{(n+2)} r_p + n r_p - \frac{n(n-1)}{2} r_p^{n+1} + \frac{(n^4 + 2n^3 - 5n^2 - 6n + 4)}{2(n+2)(n+3)} r_p^{n+3} \right)$$

$$+ a_1 J_0(i\alpha r) \qquad \text{if } 0 \le r \le r_p,$$

$$(52)$$

and the solution of steady dispersion function in the outer flow region,  $f_{ls+}(r)$  is not shown in this study as the result is complex.

Using variable separable method into Eqn (44) and Bessel function subject to the boundary conditions the most general solution of  $f_{tt}(r,t)$  is given as:

$$f_{1t}(r,t) = \sum_{m=1}^{\infty} A_m e^{-\lambda_m^2 t} J_0(\lambda_m r),$$
 (53)

where

$$A_{m} = -\frac{2}{J_{0}^{2}(\lambda_{m})} \left( \int_{0}^{r_{p}} J_{0}(\lambda_{m}r) f_{1s-}(r_{p}) + \int_{r_{p}}^{R(z)} J_{0}(\lambda_{m}r) f_{1s+}(r) \right).$$
 (54)

#### 3. Results and Discussion

## 3.1 Velocity of the Blood Flow

Variations in blood flow velocity under different variables as radius of the artery in plug flow region, height of stenosis and length of the stenosed area are studied. The variation of blood flow of velocity is compared to Dash *et al.*, [17] in order to validate the variations. Figure 3 shows the validation of current study with Dash *et al.*, [17]. The value used in order to tally Dash *et al.* [17] are P=2,  $R_0=1$ ,  $l_0=1$ , d'=0.5,  $\delta=0$ , z=0.3, and  $r_p=0.02$ . As a result, the velocity variation measured is exact.

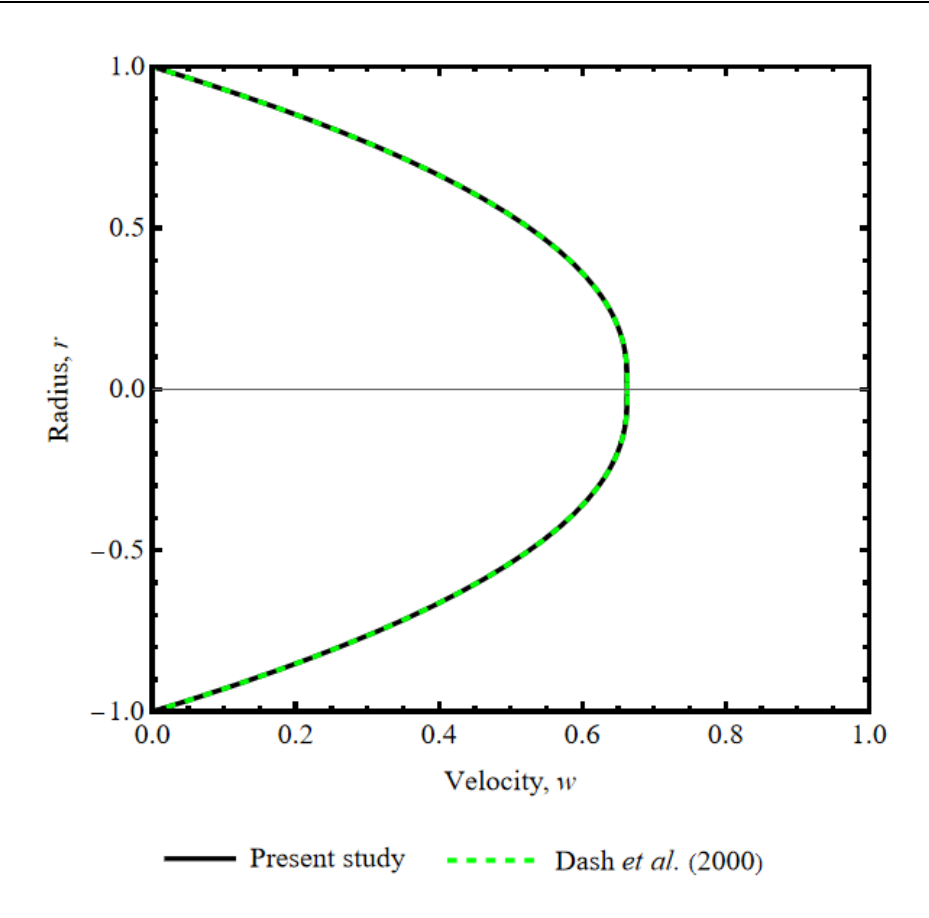
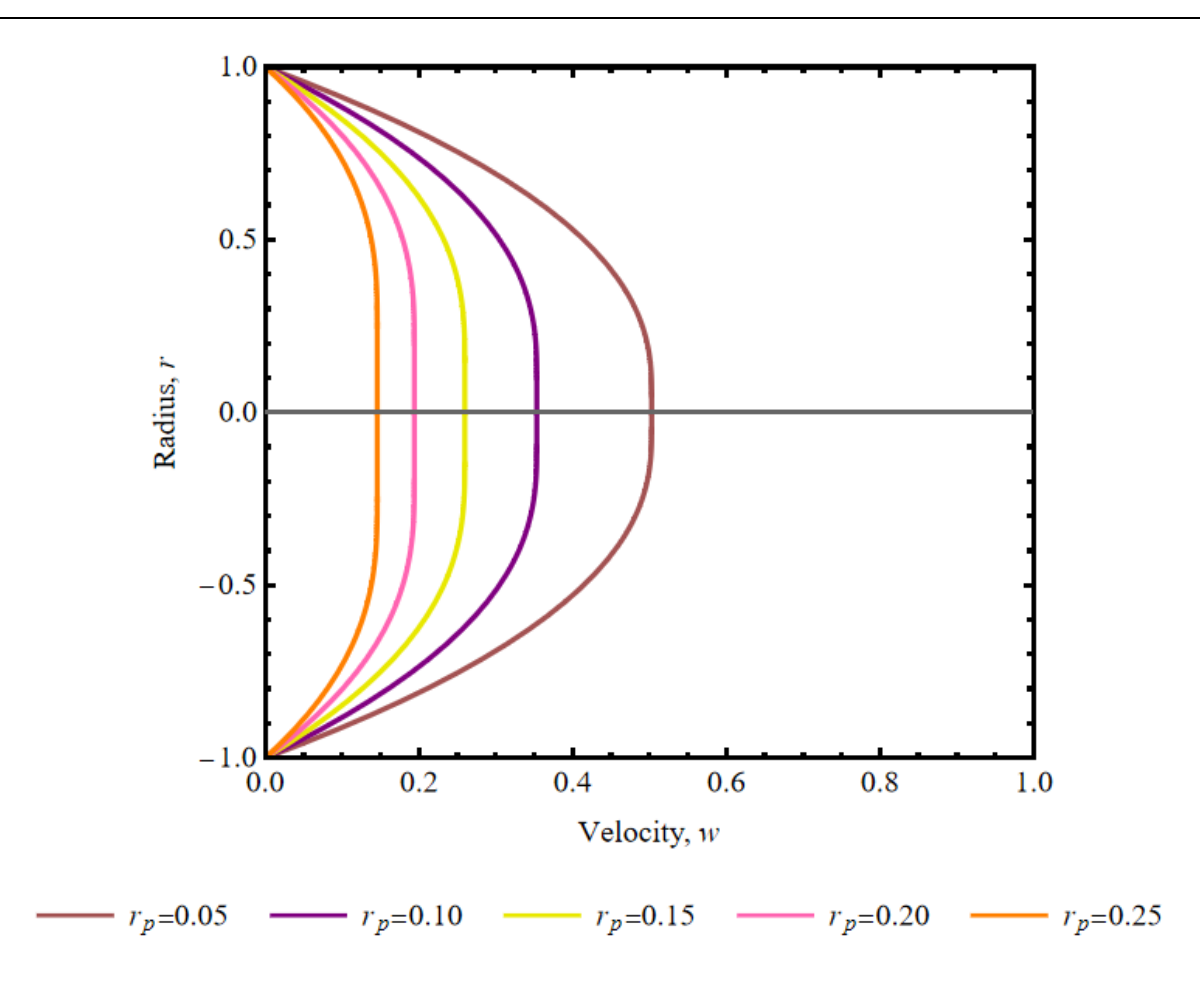


Fig. 3. Validation of present study of velocity with Dash et al., [17]

Figure 4 shows the variation of velocity, w for different values of radius of the artery in plug flow region,  $r_n$ . The focus of this figure is plug flow region, and the value studied in this graph are 0.05, 0.15, 0.20, and 0.25. The constant value 0.10, used in this figure P=2,  $R_0=1$ ,  $l_0=1$ , d'=0.5,  $\delta=0.2$  and z=0.3. From the generated graph, as the radius of the artery in plug flow region increases, the velocity of the blood flow decreases. This inverse trend attributes to the expansion of the plug core, which reduces the velocity gradient across the arterial cross-section. As the plug region becomes wider, the contribution of the shear-driven flow near the vessel wall diminishes, resulting in a lower overall flow velocity. This behavior is consistent with the rheological properties of non-Newtonian fluids, where velocity profiles are sensitive to radial changes and shear-dependent viscosity.



**Fig. 4.** Variation of velocity, w for different values of radius of the artery in plug flow region,  $r_p$ .

Figure 5 shows the variation of velocity, w for different values of height of stenosis,  $\delta$  . The focus of this figure is height of stenosis, and the value studied in this graph are 0.1, 0.2, 0.3, 0.4 and 0.5.

The constant value used in this figure are 
$$P=2$$
,  $R_0=1$ ,  $l_0=1$ ,  $d'=0.5$ ,  $r_p=0.01$  and  $z=d'+\left(\frac{l_0}{2}\right)$ 

From the generated graph, as the height of stenosis increases, the velocity of blood flow decreases. This observation is consistent with the expected hemodynamic behavior in stenosed arteries, where a greater degree of narrowing imposes higher resistance to flow. The reduction in effective cross-sectional area due to increased stenosis height limits the passage of blood, thereby diminishing the axial velocity. In the context of non-Newtonian blood behavior, this effect becomes more pronounced, as the shear-dependent viscosity further influences the velocity distribution.

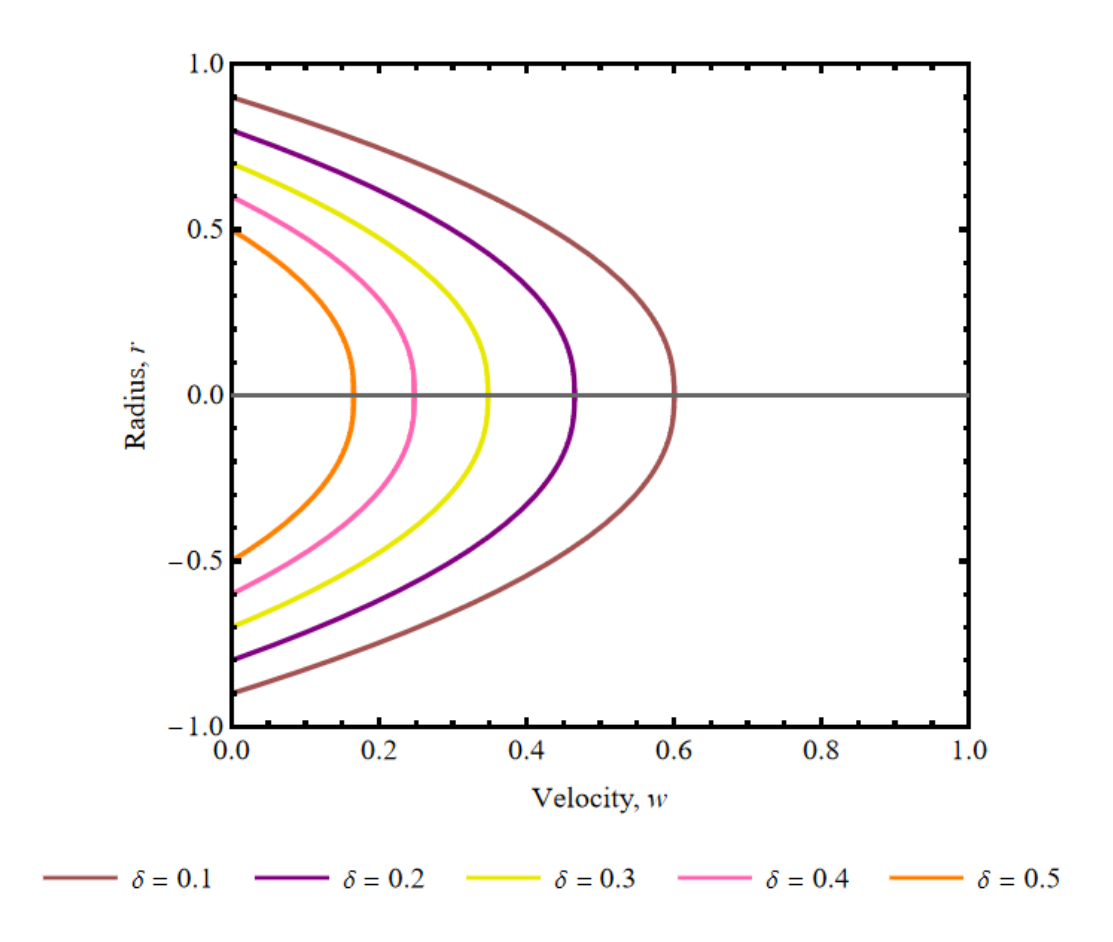


**Fig. 5.** Variation of velocity, w for different values of height of stenosis,  $\delta$ 

Figure 6 shows the variation of velocity, w for different values of length of the stenosed area,  $l_0$ . The focus of this figure is the length of the stenosed area, and the value studied in this graph are 1.0, 1.2, 1.6, 1.8 and 2.0. The constant value used in this figure are  $P=2,\ R_0=1,\ \delta=0.1,\ d'=0.5,\ r_p=0.01$  and  $z=d'+\left(\frac{l_0}{2}\right)$ . The point of study at axial axis in  $\overline{z}$ 

direction is set as  $z=d'+\left(\frac{l_0}{2}\right)$ , in order z is set at the peak of stenosis. From the generated graph,

when  $l_0$  increases, the velocity of blood flow decreases and then increases. This behavior can be interpreted as a result of the competing effects between flow restriction and pressure recovery. At shorter stenosis lengths, the narrowing dominates, causing significant resistance and reduced velocity. However, as the length extends further, the flow begins to adjust and stabilize over the longer constricted region, allowing for partial pressure recovery and a corresponding rise in velocity. This pattern reflects the complex dynamics of blood flow in elongated stenotic segments and underscores the importance of stenosis geometry, in not just height but also axial length, influencing hemodynamic performance, particularly under non-Newtonian flow conditions.

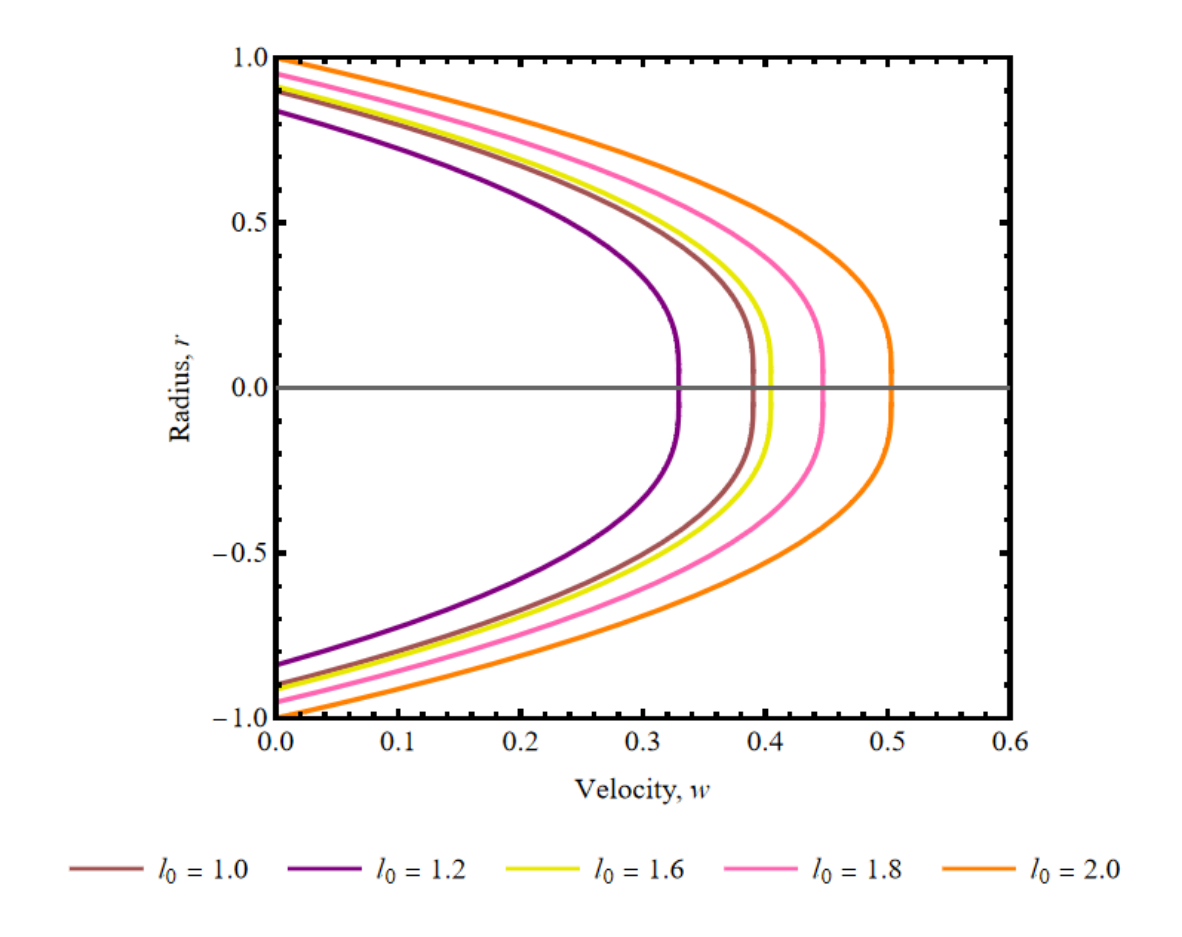


**Fig. 6.** Variation of velocity, w for different values of length of the stenosed area,  $l_0$ .

## 3.2 Dispersion Function of the Blood Flow

The dispersion function is affected under different conditions of radius of the artery in plug flow region, height of stenosis, length of the stenosed area, length from the origin till the stenosed section and the axial position. The variation of blood flow of velocity is compared to Dash et~al., [17] in order to validate the variations. Figure 7 shows the validation of current study with Dash et~al., [17]. The value used in order to tally Dash et~al., [17] are P=3,  $R_0=1$ ,  $l_0=1$ , d'=0,  $\delta=0$ , z=1,  $\alpha=0.001$  and  $r_p=0.1$ . As a result, the dispersion function variation measured is exact.

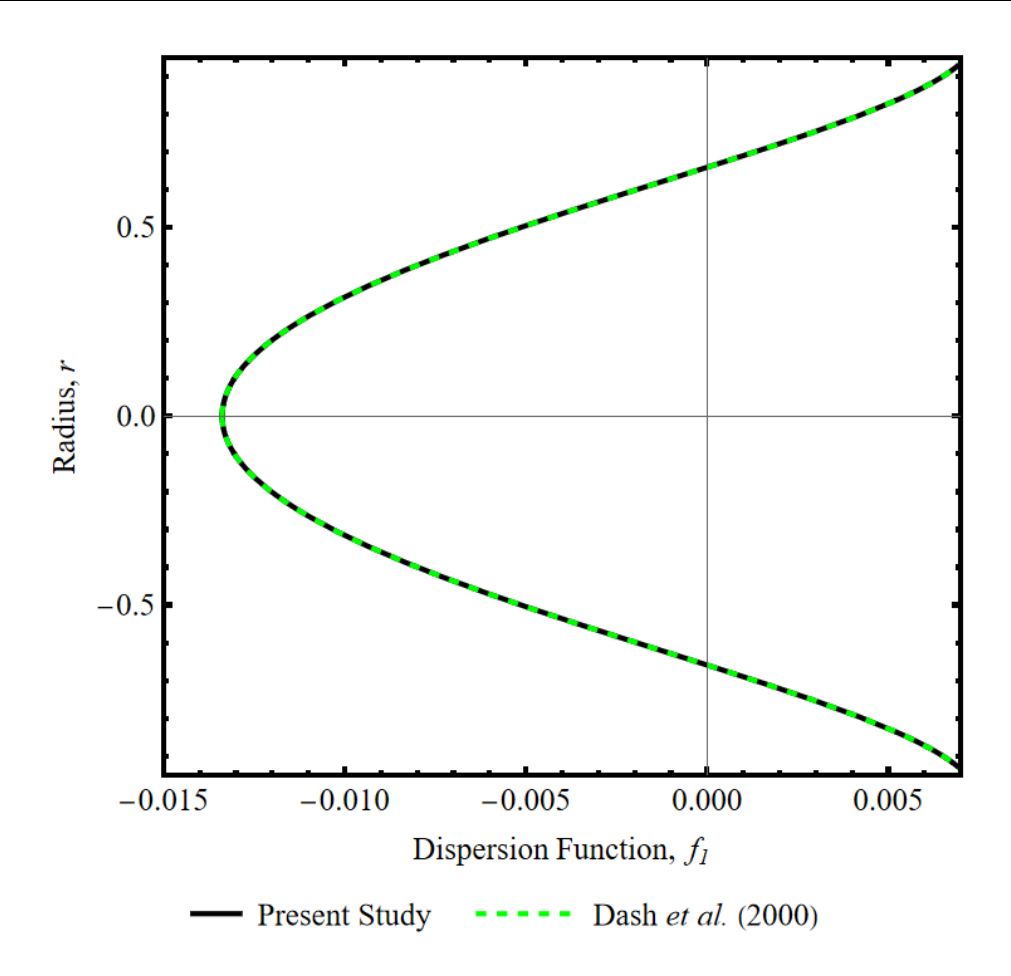
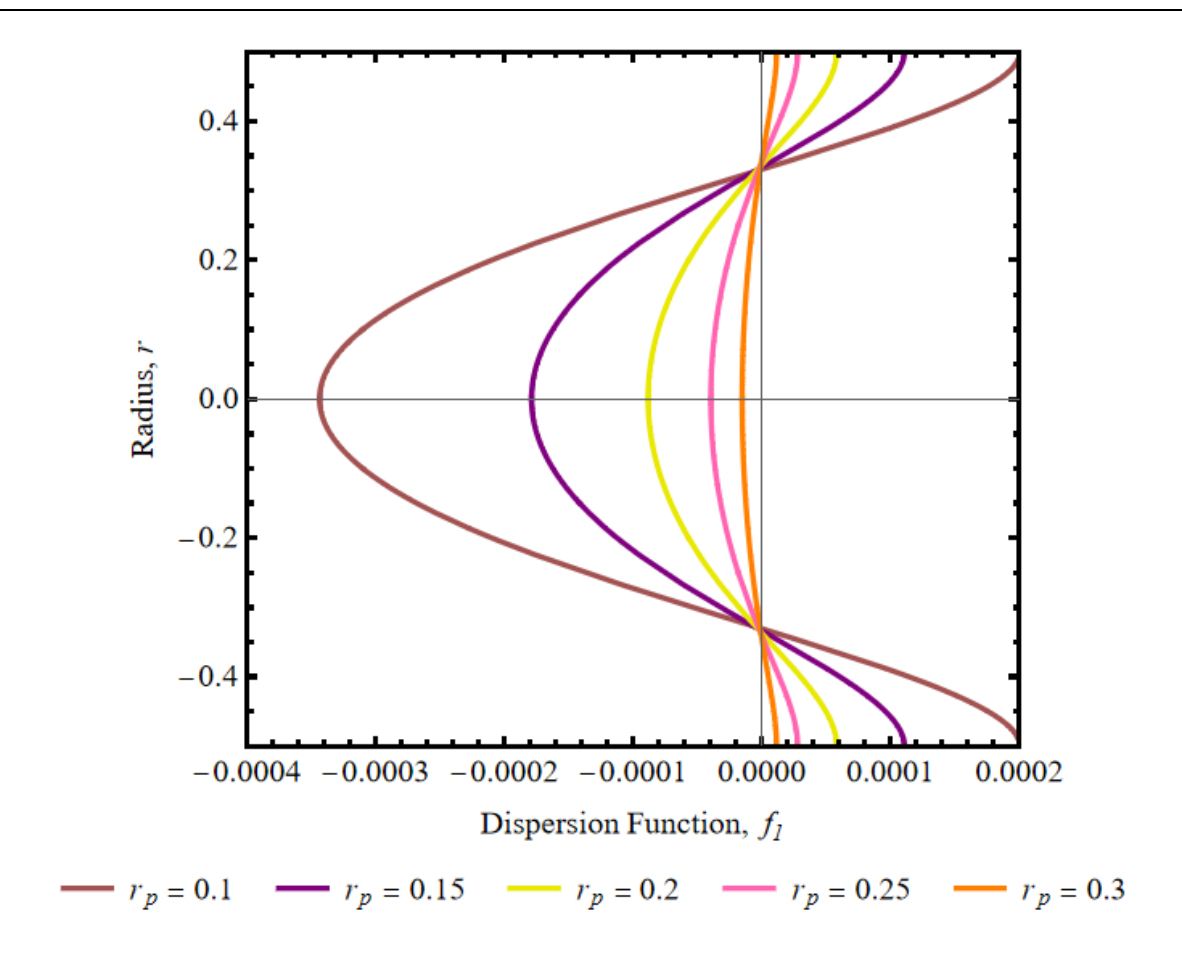


Fig. 7. Validation of present study of dispersion function with Dash et al., [17]

Figure 8 shows the variation of dispersion function,  $f_1$  for different values of radius of the artery in plug flow region,  $r_p$ . The focus of this figure is plug flow region, and the value studied in this graph are 0.1, 0.15, 0.20, 0.25 and 0.3. The constant value used in this figure are A=P=3,  $A_0=1$ , a=0.01, b=0, B=2.5,  $\alpha=0.2$ ,  $R_0=1$ ,  $l_0=1$ , d'=0.6,  $\delta=0.5$  and  $z=d+\frac{l_0}{2}$ .

From the generated graph, as the radius of the artery in plug flow region increases, the dispersion function decreases. When the plug flow region becomes wider, the spread of the solute along the artery becomes less. A wider plug region causes the flow to become more uniform, which reduces the mixing and spreading of the solute. This finding shows that the size of the plug flow region can strongly affect how substances are transported in the blood, especially in narrowed arteries.



**Fig. 8.** Variation of dispersion function,  $f_1$  for different values of radius of the artery in plug flow region,  $r_p$ .

Figure 9 shows the variation of dispersion function,  $f_1$  for different values of height of stenosis,  $\delta$ . The focus of this figure is height of stenosis, and the value studied in this graph are 0.1, 0.15, 0.20, 0.25 and 0.3. The constant value used in this figure are:

$$A = P = 3$$
,  $A_0 = 1$ ,  $a = 0.01$ ,  $b = 0$ ,  $B = 2.5$ ,  $\alpha = 0.2$ ,  $R_0 = 1$ ,  $l_0 = 1$ ,  $d' = 0.6$ ,  $r_p = 0.1$  and  $z = d + \frac{l_0}{2}$ .

From the generated graph, as the height of stenosis increases, the dispersion function in the blood flow also increases. This means that when the narrowing in the artery becomes more smaller, the spreading of solutes in the blood flow becomes greater. A higher stenosis height causes more disturbance in the flow, leading to greater mixing and uneven movement of particles. This result shows that the severity of stenosis can significantly affect how solute are distributed in the bloodstream.

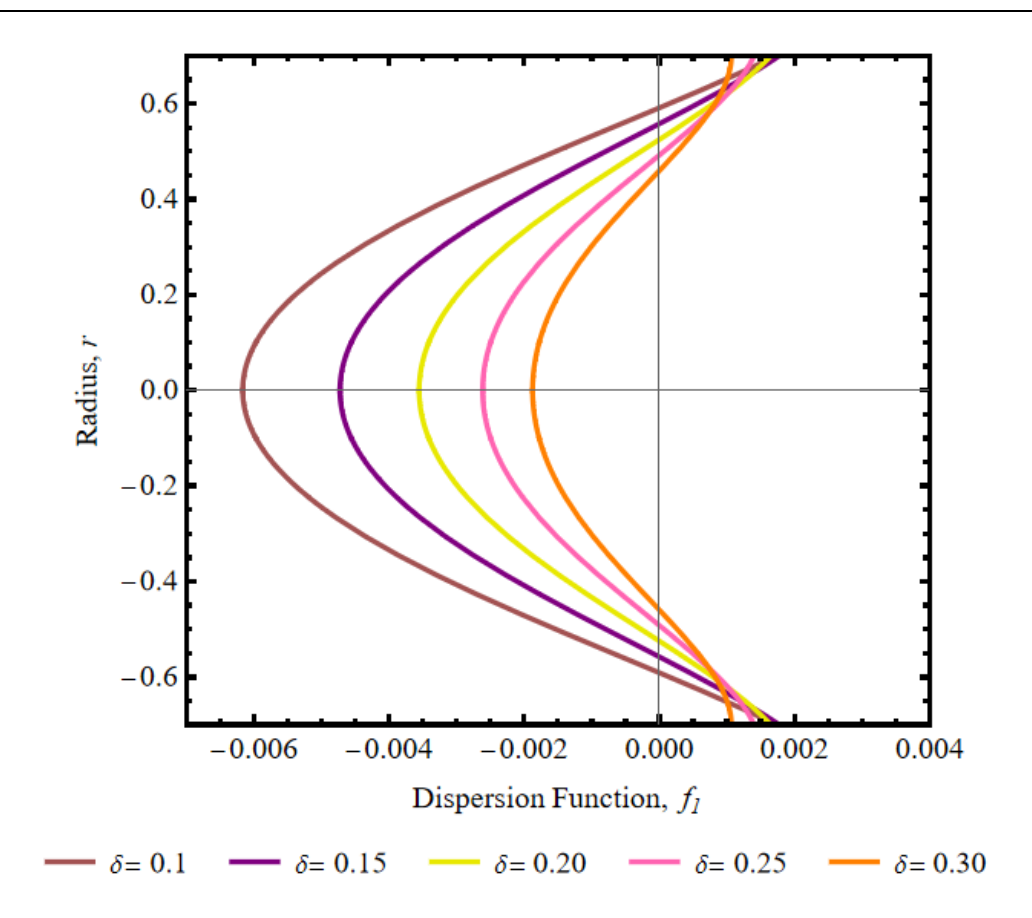


**Fig. 9.** Variation of dispersion function,  $f_1$  for different values of height of stenosis,  $\delta$ . From the generated graph, as the height of stenosis increases, the dispersion function in the blood flow also increases

Figure 10 shows Variation of dispersion function,  $f_1$  for different values of length of the stenosed area,  $l_0$ . The focus of this figure is length of the stenosed area and the value studied in this graph are 1.0, 1.5, 2.0, 2.5 and 3.0. The constant value used in this figure are A=P=3,  $A_0=1$ , a=0.01, b=0, B=2.5,  $\alpha=0.2$ ,  $R_0=1$ ,  $\delta=0.5$ , d'=0.6,  $r_p=0.1$  and z=1. The point of study at axial axis in  $\overline{z}$  direction is set to be constant at z=1, because the graph appears to constant if z is set to be at the peak of stenosis. From the generated graph, as the length of the stenosed area increases, the dispersion function in the blood flow increases, and then decreases at  $l_0=1.5$  and then increases again from  $l_0=2.0$ . This trend suggests the presence of a local minimum in the dispersion function with respect to  $l_0$ . Physically, when the stenosed length increases at first, the flow begins to stabilize within the narrowed region, reducing mixing and hence dispersion. If the length increases further, the flow may re-develop and create new mixing layers, causing dispersion to rise again.

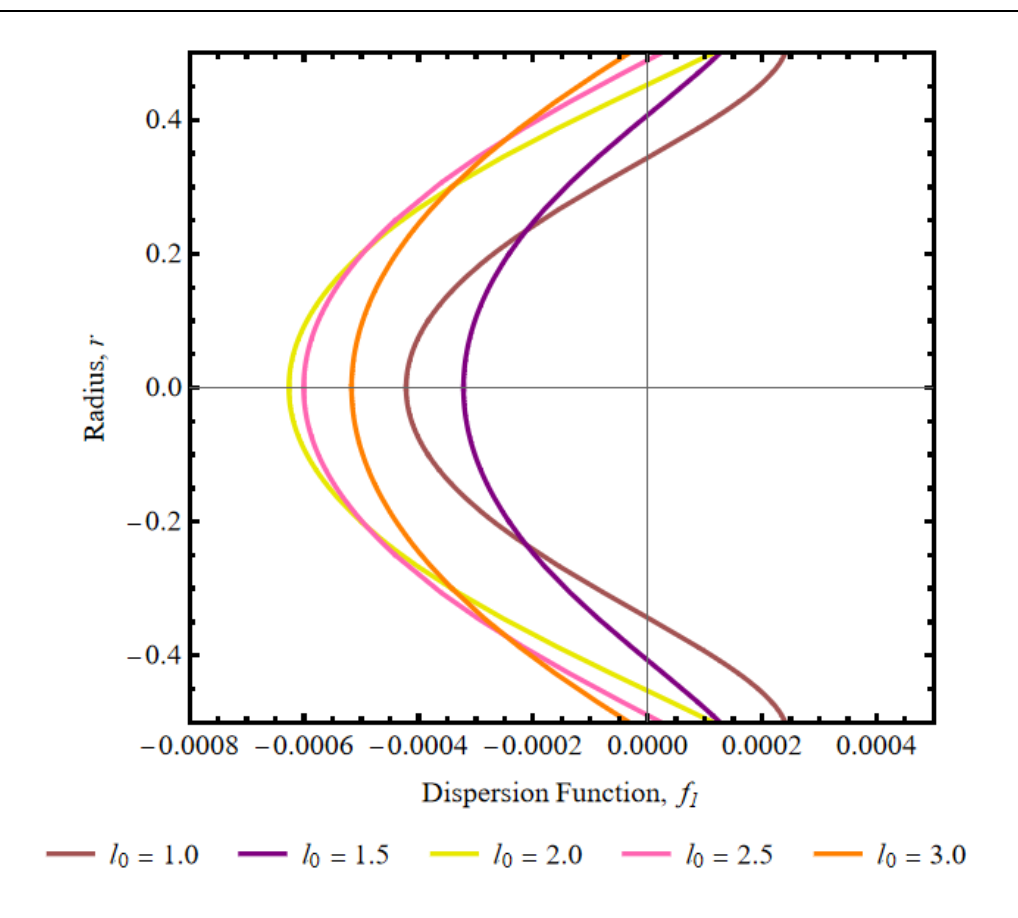


**Fig. 10.** Variation of dispersion function,  $f_1$  for different values of length of the stenosed area,  $l_0$ .

Figure 11 shows variation of dispersion function,  $f_1$  for different values of length from the origin till the stenosed section, d'. The focus of this figure is length from the origin till the stenosed section and the value studied in this graph are 0.1, 0.15, 0.20, 0.25, 0.30. The constant value used in this figure are

$$A = P = 3$$
,  $A_0 = 1$ ,  $a = 0.01$ ,  $b = 0$ ,  $B = 2.5$ ,  $\alpha = 0.2$ ,  $R_0 = 1$ ,  $\delta = 0.5$ ,  $l_0 = 1$ ,  $r_p = 0.1$  and  $z = 1$ .

This fixed position is selected because the graph remains more stable when evaluated at this point compared to the peak of stenosis. From the generated graph, as the length from the origin till the stenosed section increases, the dispersion function in the blood flow also increases. This means that when the stenosed section is located farther from the origin, the solute dispersion becomes greater. The increase in distance allows the blood flow to develop a more stable and layered profile before encountering the stenosis. As a result, when the flow reaches the narrowed section, the interaction between velocity gradients and solute particles is more pronounced, leading to greater axial dispersion.

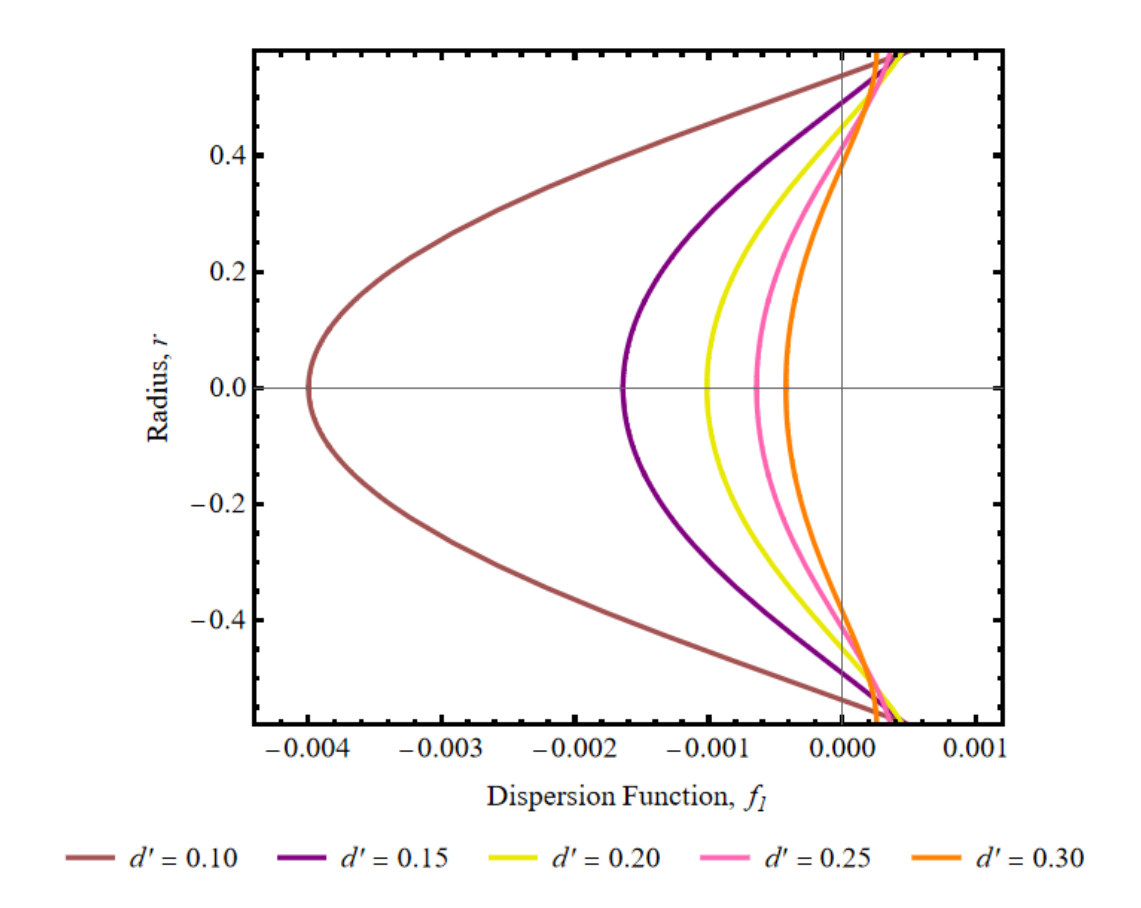


**Fig. 11**. Variation of dispersion function,  $f_1$  for different values of length from the origin till the stenosed section, d'

Figure 12 shows variation of dispersion function,  $f_1$  for different values of point at axial position, z. The focus of this figure is point at axial position and the value studied in this graph are 0.7, 0.8, 0.9, 1.0, 1.1. The constant value used in this figure are

$$A = P = 3$$
,  $A_0 = 1$ ,  $a = 0.01$ ,  $b = 0$ ,  $B = 2.5$ ,  $\alpha = 0.2$ ,  $R_0 = 1$ ,  $\delta = 0.5$ ,  $l_0 = 1$ ,  $r_p = 0.1$  and  $d' = 0.6$ .

From the generated graph, as the point at axial position increases along the axis in  $\overline{z}$  direction, the dispersion function in the blood flow increases. This trend suggests that the further downstream the observation point is located, the more the solute has dispersed. As the flow progresses through the stenosed region and beyond, the velocity gradients and flow disturbances enhance axial mixing, resulting in greater solute spread. This reflects how dispersion is cumulative along the flow path.

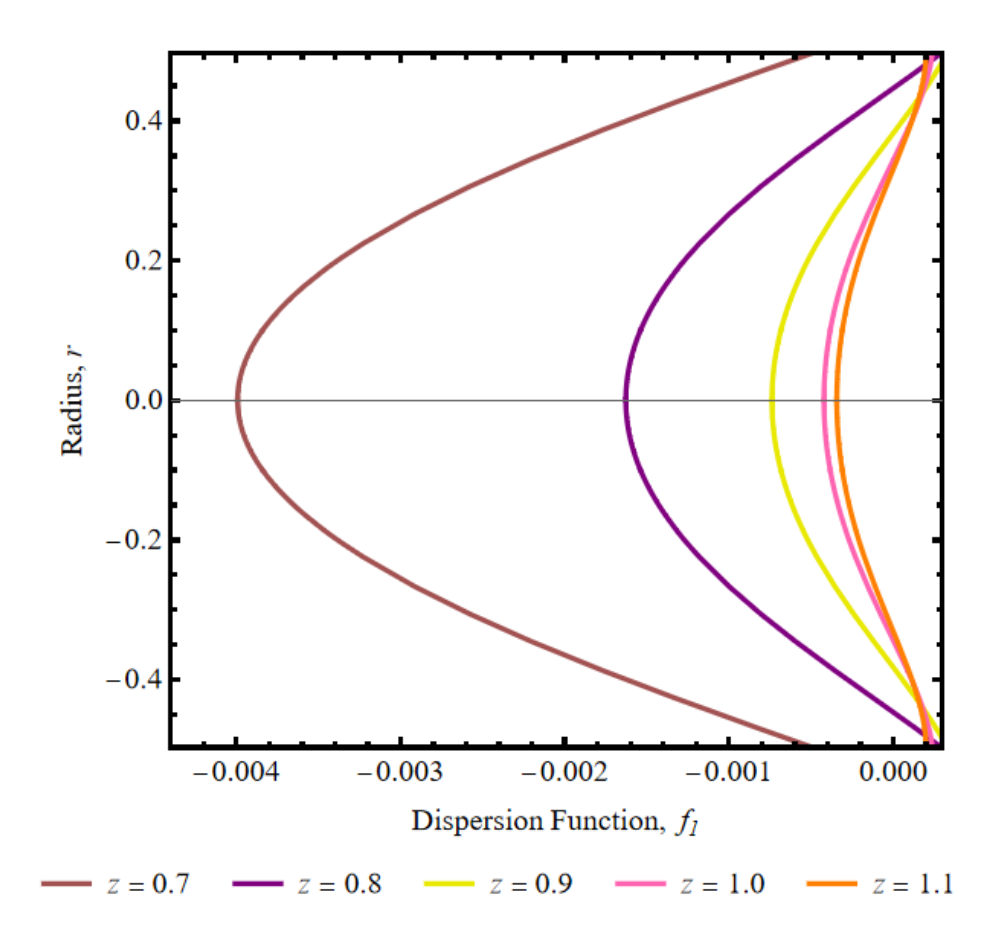


**Fig. 12.** Variation of dispersion function,  $f_1$  for different values of point at axial position, z

## 4. Conclusions

In this study, the primary objective was to investigate solute dispersion in non-Newtonian blood flow through a straight stenosed artery in the presence of a chemical reaction, using the Casson fluid model and the Generalized Dispersion Model (GDM). The velocity profile was derived by solving the governing momentum and constitutive equations in cylindrical coordinates, with appropriate boundary conditions that include velocity slip at the arterial wall. These velocity profiles were then used to analyze the dispersion function, which characterizes the axial spreading of solutes within the bloodstream. Five key parameters were examined which are the radius of the artery in the plug flow region, the height of the stenosis, the length of the stenosed area, the distance from the origin to the beginning of the stenosis, and the axial position along the artery. Symbolic computation and graphical analysis were used to assess how variations in these parameters influence both the velocity distribution and the dispersion function.

The findings indicate that increasing the plug flow region radius results in a decrease in both flow velocity and dispersion, suggesting a more uniform but less mixed flow profile. Greater stenosis height reduces the velocity while enhancing dispersion due to stronger flow disturbances. Changes in the length of the stenosed segment reveal a non-linear effect on dispersion, where it initially increases, then decreases, and subsequently rises again, reflecting the balance between flow resistance and pressure recovery along the narrowed region. When the stenosis is located further downstream from the origin, the dispersion function increases as the flow becomes more developed before encountering the constriction. Additionally, increasing the axial observation point reveals that

dispersion accumulates further along the artery. Overall, the results underscore the significant influence of arterial geometry and stenosis position on solute transport, offering valuable insights for 48modelling drug delivery, interpreting pathological flow behavior, and enhancing therapeutic strategies in vascular diseases involving non-Newtonian blood dynamics.

#### Acknowledgement

This research was supported by Universiti Teknologi Malaysia, UTMFR, PY/2024/01517/Q.J130000.3854.23H98

## References

- [1] Innes, E. A. "A brief history and overview of Toxoplasma gondii." *Zoonoses and public health* 57, no. 1 (2010): 1-7. https://doi.org/10.1111/j.1863-2378.2009.01276.x
- [2] González-Parra, Gilberto, Sharmin Sultana, and Abraham J. Arenas. "Mathematical modeling of toxoplasmosis considering a time delay in the infectivity of oocysts." *Mathematics* 10, no. 3 (2022): 354. https://doi.org/10.3390/math10030354
- [3] Flegr, Jaroslav, Joseph Prandota, Michaela Sovičková, and Zafar H. Israili. "Toxoplasmosis—a global threat. Correlation of latent toxoplasmosis with specific disease burden in a set of 88 countries." *PloS one* 9, no. 3 (2014): e90203. <a href="https://doi.org/10.1371/journal.pone.0090203">https://doi.org/10.1371/journal.pone.0090203</a>
- [4] Lv, Qing-Bo, Ao Zeng, Lin-Hong Xie, Hong-Yu Qiu, Chun-Ren Wang, and Xiao-Xuan Zhang. "Prevalence and risk factors of Toxoplasma gondii infection among five wild rodent species from five provinces of China." *Vector-Borne and Zoonotic Diseases* 21, no. 2 (2021): 105-109. https://doi.org/10.1089/vbz.2020.2658
- [5] Torgerson, Paul R., and Pierpaolo Mastroiacovo. "The global burden of congenital toxoplasmosis: a systematic review." *Bulletin of the World Health Organization* 91 (2013): 501-508. https://doi.org/10.2471/blt.12.111732
- [6] Pleyer, Uwe, Uwe Gross, Dirk Schlüter, Henrik Wilking, and Frank Seeber. "Toxoplasmosis in Germany: epidemiology, diagnosis, risk factors, and treatment." *Deutsches Ärzteblatt International* 116, no. 25 (2019): 435.https://doi.org/10.3238/arztebl.2019.0435
- [7] Turner, Matthew, Suzanne Lenhart, Benjamin Rosenthal, and Xiaopeng Zhao. "Modeling effective transmission pathways and control of the world's most successful parasite." *Theoretical population biology* 86 (2013): 50-61. https://doi.org/10.1016/j.tpb.2013.04.001
- [8] Sultana, Sharmin, Gilberto González-Parra, and Abraham J. Arenas. "A generalized mathematical model of toxoplasmosis with an intermediate host and the definitive cat host." *Mathematics* 11, no. 7 (2023): 1642. https://doi.org/10.3390/math11071642
- [9] Brandon-Mong, Guo-Jie, Nurul Asma Anati Che Mat Seri, Reuben Sunil-Kumar Sharma, Hemah Andiappan, Tian-Chye Tan, Yvonne Ai-Lian Lim, and Veeranoot Nissapatorn. "Seroepidemiology of toxoplasmosis among people having close contact with animals." *Frontiers in immunology* 6 (2015): 143. <a href="https://doi.org/10.3389/fimmu.2015.00143">https://doi.org/10.3389/fimmu.2015.00143</a>
- [10] Olopade, Isaac A., I. T. Mohammed, M. E. Philemon, T. O. Akinwumi, S. O. Sangoniyi, G. A. Adeniran, S. O. Ajao, and S. O. Adewale. "A Study of a Class Continuous SIR Epidemic Model with History." *Journal of Basics and Applied Sciences Research* 2, no. 1 (2024): 54-60. <a href="https://doi.org/10.33003/jobasr-2024-v2i1-28">https://doi.org/10.33003/jobasr-2024-v2i1-28</a>
- [11] Deng, Huifang, Rachel Cummins, Gereon Schares, Chiara Trevisan, Heidi Enemark, Helga Waap, Jelena Srbljanovic et al. "Mathematical modelling of Toxoplasma gondii transmission: A systematic review." *Food and waterborne parasitology* 22 (2021): e00102.https://doi.org/10.1016/j.fawpar.2020.e00102
- [12] Ayoade, A. A., T. Oyedepo, and S. Agunbiade. "Mathematical modeling of Toxoplasma gondii between the environment and cat population under vaccination and sanitation." *Journal of Fractional Calculus and Applications* (*JFCA*) 14, no. 1 (2023): 75-87.
- [13] Kamran, Ayesha, Shah Zeb, Siti Ainor Mohd Yatim, and Muhammad Rafiq. "Numerical Investigation of a Chlamydia Epidemic Model." *Malaysian Journal of Fundamental and Applied Sciences* 21, no. 2 (2025): 1808-1822. <a href="https://doi.org/10.11113/mjfas.v21n2.4085">https://doi.org/10.11113/mjfas.v21n2.4085</a>
- [14] Ijaz Khan, M., Kamel Al-Khaled, Ali Raza, Sami Ullah Khan, Jiyan Omar, and Ahmed M. Galal. "Mathematical and numerical model for the malaria transmission: Euler method scheme for a malarial model." *International Journal of Modern Physics B* 37, no. 16 (2023): 2350158. <a href="https://doi.org/10.1142/s0217979223501588">https://doi.org/10.1142/s0217979223501588</a>
- [15] Singh, Ravindra, Omwati Rana, Yogesh Kumar Sharma, and Shiv Shankar Gaur. "Numerical Approximation Methods and Comparison with RK-4 Method for a Linear Differential Equation with Initial Conditions Using Scilab 6.1." *Peerreviewed, Partially Open-access Journal* 1, no. 6 (2024): 471. https://doi.org/10.63015/5c-2447.1.6

- [16] Mickens, Ronald E., and Talitha M. Washington. "A note on an NSFD scheme for a mathematical model of respiratory virus transmission." *Journal of Difference Equations and Applications* 18, no. 3 (2012): 525-529.https://doi.org/10.1080/10236198.2010.515590
- [17] Khoshnaw, Sarbaz HA, Rizgar H. Salih, and Sadegh Sulaimany. "Mathematical modelling for coronavirus disease (COVID-19) in predicting future behaviours and sensitivity analysis." *Mathematical Modelling of Natural Phenomena* 15 (2020): 33. <a href="https://doi.org/10.1051/mmnp/2020020">https://doi.org/10.1051/mmnp/2020020</a>